Beam Switching Reflectarray Monolithically Integrated With RF MEMS Switches

Omer Bayraktar, Ozlem Aydin Civi, *Senior Member, IEEE*, and Tayfun Akin, *Member, IEEE*

***Abstract*—A reflectarray antenna monolithically integrated with 90 RF MEMS switches has been designed and fabricated to achieve switching of the main beam. Aperture coupled microstrip patch antenna (ACMPA) elements are used to form a 10×10 element reconfigurable reflectarray antenna operating at 26.5 GHz. The change in the progressive phase shift between the elements is obtained by adjusting the length of the open ended transmission lines in the elements with the RF MEMS switches. The reconfigurable reflectarray is monolithically fabricated with the RF MEMS switches in an area of 42.46 cm^2 using an in-house surface micromachining and wafer bonding process. The measurement results show that the main beam can be switched between broadside and 40° in the H-plane at 26.5 GHz.**

***Index Terms*—Reflectarray antennas, reconfigurable antennas, micro-electro-mechanical systems (MEMS) switches, microstrip antennas.**

I. Introduction

REFLECTARRAYS are mostly planar printed surfaces that direct the incident electromagnetic field radiated from a feed horn antenna to a desired direction. Microstrip reflectarrays have many advantages compared to parabolic reflectors and electronically scanned phased array antennas. Microstrip reflectarrays have lower weight and smaller size compared to parabolic reflector antennas; furthermore, they allow electronic beam scanning. Reflectarrays do not contain a complex feed system as in phased array antennas; they employ feeding through free space which eliminates the losses of a microstrip feed network that limits the performance of high-gain millimeter wave arrays [1].

In reflectarrays, the phase of the reflected field from each element is adjusted so that the main beam can be directed to a desired direction. In the literature, there are several configurations proposed to control the reflection phase [2], such as patch antennas with variable-length stubs [3], variable-length cross dipoles [4], and patch antennas with variable size [5]. Most of the reflectarrays available in the literature have fixed beams. Recently, there is a growing interest to design and implement beam steering reflectarrays. The electronically beam scanning reflectarrays are obtained by using reconfigurable components and materials to control the reflection phase difference between the antenna elements, such as tunable dielectrics [6], [7], varactor diodes [8]–[12], PIN diodes [13], [14], and various micro-electro-mechanical systems (MEMS) structures (such as micro-motors), or RF MEMS switches [15], [16], [18]–[26]. In [6] and [7], the dielectric constant of the nematic liquid crystal under each patch antenna in the reflectarray is changed by applying a DC voltage to steer the beam. Although there is no need for a complex biasing network for such a reflectarray, the response time of a liquid crystal is very slow, limiting its applications. The phase of the reflected field can dynamically be adjusted using semiconductor varactor diodes that are placed in various configurations, such as to control the slot susceptance of patches [8], to control the surface impedance [9], to load a transmission line stub in aperture coupled patches [10], to obtain capacitive loading of hollow patches [11], and to adjust the resonant frequency of microstrip patches [12]. The phase of the reflected field can also be adjusted using PIN diodes to control the length of a short circuited stub [13] or using both varactor and PIN diodes to change the current distribution on a cross shaped microstrip loop [14].

Recent reconfigurable reflectarrays [15], [16], [18]–[26], and lens arrays [27] prefer RF MEMS components (such as switches, varactors, and phase shifters), since electrostatically actuated RF MEMS components provide almost zero DC power consumption, low insertion loss, high isolation, and linear characteristics compared to solid state switches. Although RF MEMS switches and other components have drawbacks in terms of reliability and low switching speed, as presented in a detailed discussion on performance comparison of different switch technologies in [28], they provide several advantages in mm-wave reconfigurable array applications. The most important advantage is that RF MEMS switches and other components can be easily manufactured monolithically with antennas on the same substrate. The monolithic integration is very important in the realization of reconfigurable antenna and array applications especially at mm-wave frequencies, because hybrid integration would be very complicated due to the size limitations at the mm-wave frequencies. Furthermore, losses increase due to the use of several connecting wire bonds in the case of hybrid integration.

Most of the MEMS reconfigurable reflectarray studies in the literature are limited by design and implementation of unit cell

Manuscript received March 19, 2010; revised May 18, 2011; accepted August 08, 2011. Date of publication October 20, 2011; date of current version February 03, 2012. This work was supported in part by the Scientific and Technological Research Council of Turkey (TUBITAK-EEEAG-104E041), by the Turkish State Planning Organization (DPT), and by the AMICOM (Advanced MEMS For RF and Millimeter Wave Communications) Network of Excellence under the 6th Framework Program of the European Union.

O. Bayraktar and O. Aydin Civi are with the Department of Electrical and Electronics Engineering, Middle East Technical University, Ankara 06800, Turkey (e-mail: bomer@metu.edu.tr; ozlem@metu.edu.tr).

T. Akin is with the Department of Electrical and Electronics Engineering, Middle East Technical University, Ankara 06800, Turkey, and also with the METU-MEMS Center, Ankara 06800, Turkey (e-mail: tayfuna@metu.edu.tr).

Color versions of one or more of the figures in this paper are available online at http://ieeexplore.ieee.org.

Digital Object Identifier 10.1109/TAP.2011.2173099

structures. Some examples of unit cells are a stub loaded patch antenna rotated by micro-machined motors [16], series of half dipoles connected to the periphery of a circular metal layer by means of diodes [17] or MEMS switches [18], [19], split ring elements with MEMS switches to obtain a phase shift by rotation of elements for circular polarization applications, [20], variable-length dipoles using electrically [21] or optically [22] actuated MEMS switches, ring elements loaded with MEMS capacitors [23], and patches loaded by MEMS varactors [24]. In [24], it has been demonstrated that, by using MEMS varactors instead of semiconductor counterparts to load patches in [12], losses can be reduced significantly, and nonlinear effects due to semiconductor diodes can be eliminated. There are a few monolithically fabricated MEMS reflectarray studies in which whole reflectarray structures have been designed but their prototypes have been fabricated either without MEMS switches, or with frozen MEMS switches [25], [26]. To the authors' knowledge, there are no monolithically integrated MEMS reconfigurable reflectarrays presented in the literature. Thus, this study presents the first monolithically fabricated reconfigurable reflectarray employing a large number of functional RF MEMS switches distributed over a large wafer area.

The reflectarray in this study is composed of aperture coupled microstrip patch antenna (ACMPA) elements, and reconfigurability in the main beam direction is obtained with series RF MEMS switches placed on open-ended transmission lines of the ACMPA elements. Section II presents details of the reflectarray design. Section III explains design of the series RF MEMS switch structure in the reflectarray and examines effects of bias lines on the performance. Section IV describes fabrication steps of a 10×10 reconfigurable reflectarray antenna monolithically produced with the RF MEMS switches and discusses the fabrication challenges and imperfections. Finally, Section V gives simulation and measurement results.

II. Reconfigurable Reflectarray Antenna Structure and Design Procedure

The ACMPA elements shown in Fig. 1 are linearly spaced with half a free space wavelength, $\lambda_0/2$, in both directions to form a 10×10 reflectarray at 26.5 GHz. Reconfigurability is achieved using series RF MEMS switches monolithically integrated with the transmission lines of the ACMPA elements. Then, phase center of the pyramidal feed horn antenna having aperture dimensions 2.212 cm $\times$ 2.212 cm is positioned at $\mathrm{x} = 0$ cm, $\mathrm{y} = -9.4$ cm, and $\mathrm{z} = 20$ cm with respect to the center of the reflectarray. Using the procedure described in [1], required reflection phase values from the elements of the reflectarray are calculated to direct the main beam toward broadside and 40° in the H-plane. For the ith element, the reflection phase values to direct the main beam to the broadside and 40° are denoted as Ψ_{i1} and Ψ_{i2}, respectively. Note that, $\Psi_{i1} = \Psi_{i2}$ for the elements in the first column, because the first column is taken as a reference in the calculation of the progressive phase shifts.

Two mostly used approaches to achieve required phase of reflected field from reflectarray cells in linearly polarized applications are (i) tuning of resonance of elements either by manipulating dimensions or by reactive loading of the elements [12], [23], [29] and (ii) using a separate phase shifter, as in the reflectarray presented in this paper [15], [25]. The reflectarray cells having a phase shift control mechanism based on resonance tuning possess very low losses in the operation band except around the resonance frequencies of structures [12]. However, the reflectarray cells with separate phase shifters have relatively higher losses due to the insertion loss of a phase shifter, which is generally larger than the insertion loss of a switch or a capacitor. On the other hand, the use of a separate phase shifter simplifies the design and analysis of a reflectarray, since the radiating structures of all cells are identical.

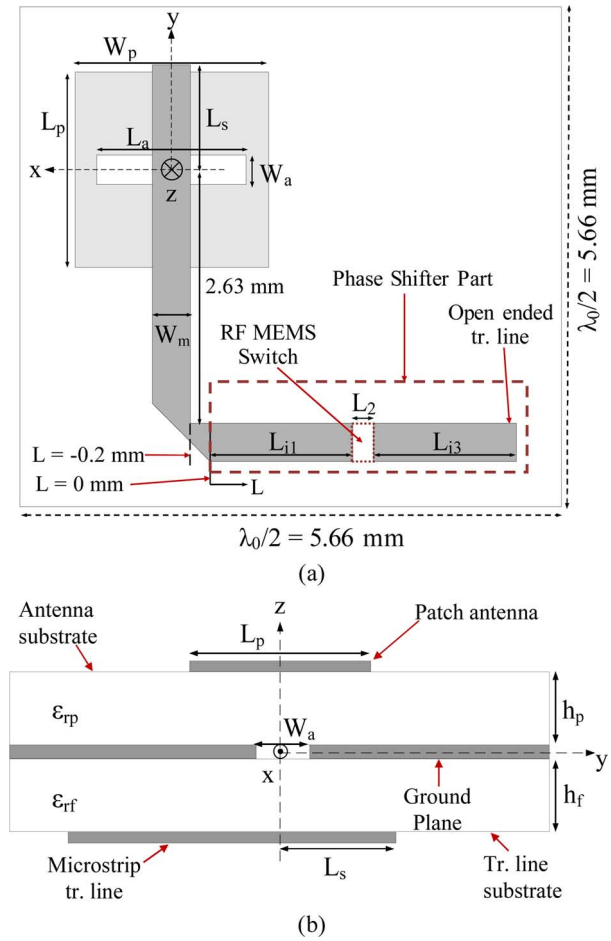

Fig. 1. (a) Backside and (b) cross-sectional views of the aperture coupled microstrip patch antenna element used in the reconfigurable reflectarray.

The ACMPA reflectarray configuration has many advantages as well as drawbacks over the configuration where the phase shifter and antenna are on the same layer. One of the main advantages is that the microstrip transmission line and patch antenna are printed on different substrates separated by a common ground plane, and hence, a large space on the microstrip line side is obtained to place bias lines for MEMS switches and/or some active components if needed. Furthermore, the length of each transmission line in the reflectarray can be extended to obtain several multiples of 360° phase delay to eliminate the bandwidth limitation due to differential spatial phase delays [30] so that the bandwidth of the reflectarray is determined by the element bandwidth. Another advantage is the flexibility of choosing two separate substrates for the patch antenna and transmission line, for example, a high dielectric substrate for the

phase shifters can be chosen to obtain large phase shifts, while the microstrip patch antenna can be printed on a low dielectric substrate in order to increase the element bandwidth, radiation efficiency, and steering range without scan blindness. One other advantage is that the spurious radiation due to the transmission line, RF MEMS switch, and bias lines is backwards and does not disturb the radiation pattern. Besides, the spurious radiation, and hence the power loss, can be eliminated by placing an additional ground plane at a specific distance from the microstrip lines at the back. The final advantage of the multilayer structure over the single layer structure is the simplicity of the design as far as the biasing scheme is concerned, as the effects of the bias lines and RF MEMS switches on the radiation pattern in the single layer structure should be taken into account in the design stage. On the other hand, the main drawback of multilayered reflectarray structures is the fabrication complexity and cost, which can be tolerated considering their advantages.

The principle of operation of the ACMPA element in the reflectarray is as follows. A patch antenna printed on an antenna substrate receives linearly polarized electromagnetic wave. Then, the electromagnetic wave couples to the microstrip line printed on a feed substrate by means of an aperture on the ground plane between two substrates. Since the microstrip transmission line is open ended, the wave reflects back and couples to the patch antenna using the aperture on the ground plane. The distance that the wave propagates on the transmission line determines the phase of the reflected field. Hence, two sets of transmission line lengths are needed for each element in the reflectarray to switch the main beam between the broadside and 40°, respectively. Therefore, there is one RF MEMS switch per each element, which corresponds to 1-bit of control resulting in two beam states. The number of beam states can be increased by placing 3 or 5 bit MEMS phase shifters on the transmission lines. This will increase the complexity of the biasing scheme and the loss; however, the concept of having reconfigurability using MEMS will still remain valid.

To determine the transmission line length of the element for a given reflection phase value, the graph that relates the reflection phase to the transmission line length, namely, the phase design curve must be obtained. To calculate the phase design curve, mutual couplings with the neighboring elements are taken into account by the infinite array assumption. The unit cell has been simulated as an infinite array using the periodic boundary conditions in the Ansoft High Frequency Structure Simulator (HFSS). The element spacing is half a free space wavelength ($\lambda_0 = 11.32$ mm) in both directions, thus the unit cell has a dimension of 5.66 mm × 5.66 mm. A glass substrate of thickness $h_p = h_f = 0.5$ mm, dielectric constant $\varepsilon_{rp} = \varepsilon_{rf} = 4.6$ and $\tan\delta = 0.005$ is used for both the patch and microstrip line substrates. Initial dimensions of the reflectarray element are determined by considering the element as a single radiating antenna, i.e., by matching the input impedance of a patch to the characteristic impedance of the transmission line. Then, the reflectarray element dimensions are optimized to have a linear phase design curve at 26.5 GHz by exciting the unit cell with a y-polarized plane wave normally incident to the array surface and by calculating the phase and magnitude of the field reflected from the unit cell using HFSS for each value of L incremented in the direction shown in Fig. 1(a). The ACMPA dimensions are determined as $W_p = 2.03$ mm, $L_p = 2.03$ mm, $W_m = 0.4$ mm, $W_a = 0.3$ mm, $L_a = 1.55$ mm, and $L_s = 1.1$ mm. Then, for comparison, the microstrip line of width $W_m = 0.4$ mm on the glass substrate is simulated in HFSS to obtain the ideal phase characteristics of the microstrip line at 26.5 GHz. As seen in Fig. 2, a very good agreement between the phase design curve and the ideal phase characteristics of the transmission line is obtained at 26.5 GHz. The magnitude of the reflected wave changes between −1.42 dB and −3.64 dB at 26.5 GHz as a function of L. Hence, the average value of all losses in the unit cell is 2.53 dB where the conductor losses are 0.4 dB and the dielectric losses are 1.1 dB on average. The remaining 1.03 dB is the back radiation loss. The main loss mechanisms in the unit cell are the dielectric and back radiation losses which can be eliminated by using a lower dielectric constant substrate and by placing an additional ground plane at the back. Both this non-uniform magnitude response and the amplitude variation of the incident field affect the radiation pattern, especially the side lobes. As the frequency deviates from 26.5 GHz, the linearity of the phase design curve is lost, and the range of the magnitude variation increases as shown by the simulation results in Fig. 2. Since the phase curves for different frequencies are not parallel to each other, the operational bandwidth of this reflectarray is narrow. The bandwidth of the reflectarray is discussed in detail in Section V using the measurement results.

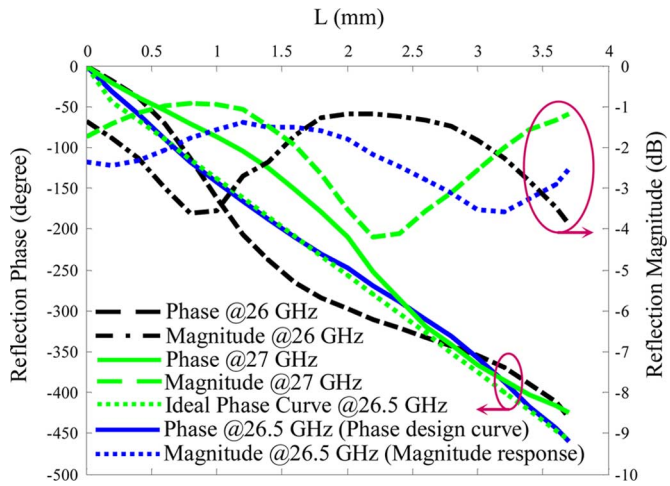

Fig. 2. The phase and magnitude curves of the unit cell for different frequencies for the normal incidence, and the ideal phase curve @26.5 GHz.

The electromagnetic wave radiated from the feed antenna does not reach all elements of the reflectarray with the same angle of incidence, and the maximum angle of incidence occurs for the elements at the edges of the reflectarray. The maximum value of the incidence angle θ_i to an element on the designed reflectarray surface is 30°, which corresponds to the worst case illumination in both E and H-planes ($\phi_i = 90°$ and $\phi_i = 0°$, respectively). In Fig. 3, the phase and magnitude curves are plotted for the worst case incidence angle in both E and H-planes and compared with the ones for the normal incidence. It is observed that the magnitude and phase curves are not affected much with the change in the incidence angle. Hence, the phase curve for the normal incidence is a good approximation for calculating the transmission line lengths.

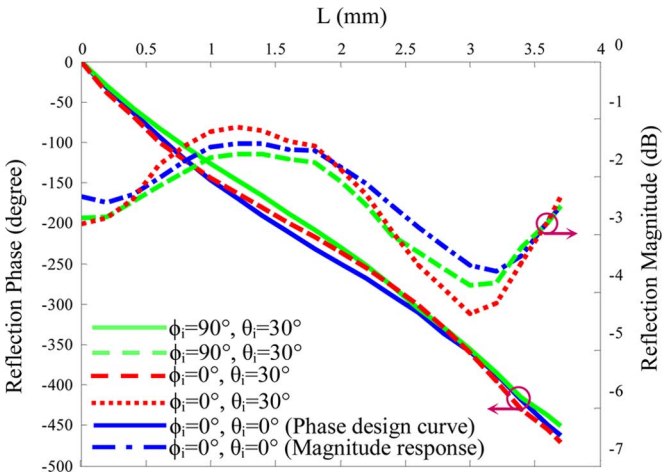

Fig. 3. The magnitude and phase responses of a y-polarized plane wave for different angles of incidence@26.5 GHz.

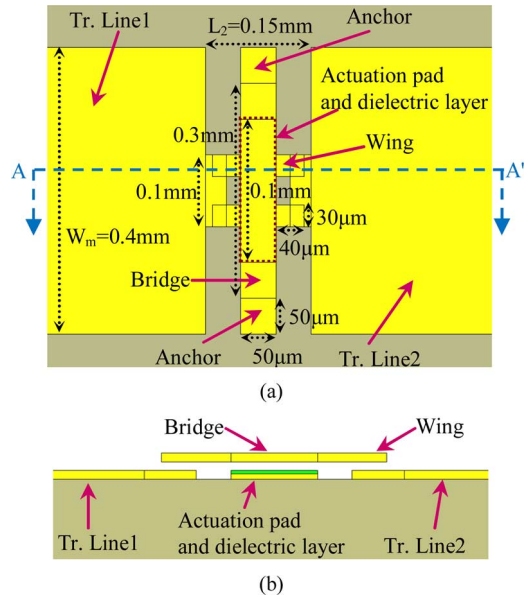

Fig. 4. (a) Top and (b) A-A′ cross-sectional views of the series RF MEMS switch.

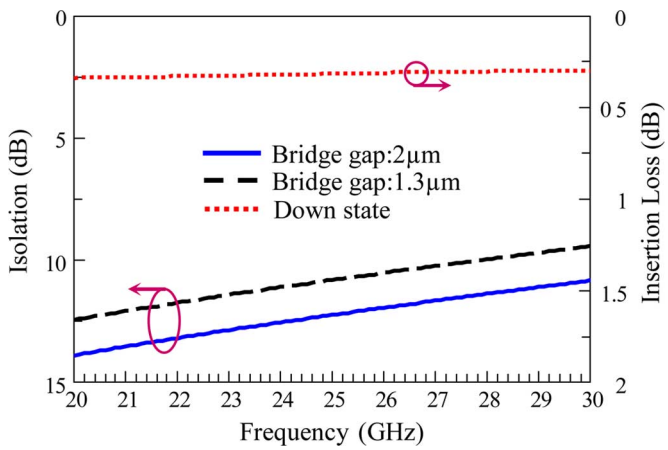

Fig. 5. The simulation results of the series RF MEMS switch.

Although all the patches on the feed side have the same size, the lengths of the transmission lines are not identical. Once the transmission line lengths are determined from the phase design curve, series ohmic contact RF MEMS switches of length L_2 can be implemented between the transmission lines of length L_{i1} and L_{i3} to switch between two transmission line lengths for all the elements, which enable the main beam to switch between the broadside and 40°. For the ith element, the transmission line lengths corresponding to Ψ_{i1} and Ψ_{i2} are denoted as L_{i1} and $L_{i1} + L_2 + L_{i3}$ in Fig. 1(a), respectively. When we consider the phase shifter part in Fig. 1(a), the open ended transmission line of length L_{i3} is connected to the microstrip transmission line of length L_{i1} through the series capacitance introduced by the RF MEMS switch. When the RF MEMS switch is in the up state, the phase shifter has a resonance for some values of L_{i3} due to imperfect isolation of the RF MEMS switch. Hence, for those values of L_{i3}, it is impossible to obtain the required phase shift values Ψ_{i1} by the transmission line of lengths L_{i1}. For this reason, the RF MEMS switches in the columns 4, 7, and 10 are kept in the down state, i.e., the overall lengths of the transmission lines are $L_{i1} + L_2 + L_{i3}$ for those elements, to achieve the phase shift values Ψ_{i1}, while the switches on the other columns are in the up state. The states of the RF MEMS switches are reversed to obtain the phase shift values Ψ_{i2}.

III. Series RF MEMS Switch and Bias Lines

We considered both shunt and series switch configurations to change the length of the microstrip line [15]. The series switch is preferred due to both size considerations and the fact that the unit cell with the series switch results in better phase design curve characteristics. The series ohmic contact RF MEMS switch used in the reflectarray is the bridge with wings type structure between two transmission line segments as shown in Fig. 4. When the switch is actuated by an applied DC voltage between the actuation pad and the bridge, it connects two physically separated transmission lines pieces named as *Tr. Line1* and *Tr. Line2*. The width of the interconnection region is reduced compared to the transmission line width to improve the isolation characteristics.

Fig. 5 shows the simulation results of the series RF MEMS switch. The insertion loss of the designed switch is less than 0.5 dB, and the isolation is better than 10 dB, which are acceptable results at the frequency of interest. The switch is fabricated using the process steps given in Section IV. The surface profile measurements on the fabricated switches show that the spacing between the transmission lines and the wings of the bridge is not 2 μm as designed but 1.3 μm, due to the residual stress of the metal bridge. To see the effect of reduced spacing on isolation, simulations have been performed for a 1.3 μm gap height. When the bridge gap becomes a 1.3 μm, the isolation is still better than 10 dB between 20–28 GHz frequency band as can be seen in Fig. 5. In order to see the effect of the bridge gap in the design, the radiation pattern simulations of the reflectarray for a 2 μm and a 1.3 μm gap heights are compared. It is observed that only the side lobe levels are affected by a few dB. When the main beam is directed to the broadside, the largest deviation of about 4 dB occurs in the side lobe around 40°. This is due to the fact that most of the switches in the broadside operation are

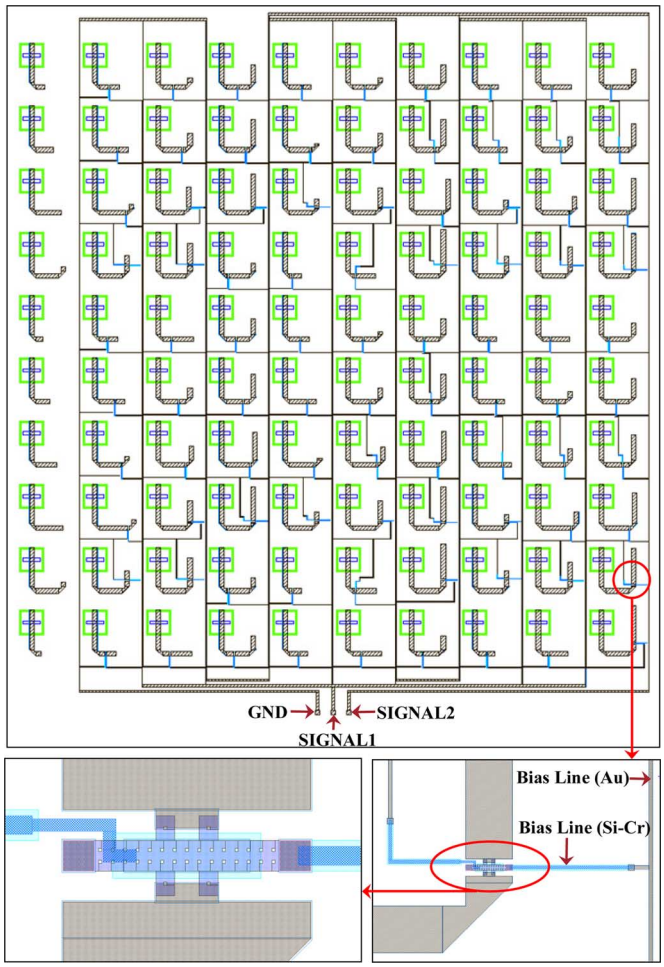

Fig. 6. Mask layout of a 10×10 reflectarray with the RF MEMS switches.

in their up states, thus the change in the up state bridge height becomes significant.

Fig. 6 shows the layout of the overall reflectarray prototype with bias lines. The bias lines used to actuate the switches have two parts: one is composed of a sputtered gold (Au) layer and the other is composed of a sputtered silicon-chromium (Si-Cr) layer. The actuation mechanism of the series switch can be modeled as a series RC circuit where the Si-Cr layer is modeled as a resistance, and the path between the bridge and actuation pad is modeled as a capacitance. In order to have a reasonable switching time, the time constant should be reduced. So, the entire bias line scheme can be composed of the sputtered gold having high conductivity. But this time, the mutual coupling between the Au bias line and microstrip line increases, and the switch performance is disturbed. In order to avoid these adverse effects, the Au bias lines are connected to the resistive bias lines composed of the sputtered Si-Cr at an average distance of 1500 μm before the switch and the transmission line, and the conductivity of the Si-Cr layer $(\sigma_{\text{Si-Cr}})$ is optimized to be 10,000 S/m.

To see the effect of the Au bias lines, the phase design curve and the amplitude response are recalculated when there are both vertical and horizontal Au bias lines in the unit cell. Then these results are compared with the ones obtained without a bias line as shown in Fig. 7. As can be seen in Fig. 7, the Au bias lines

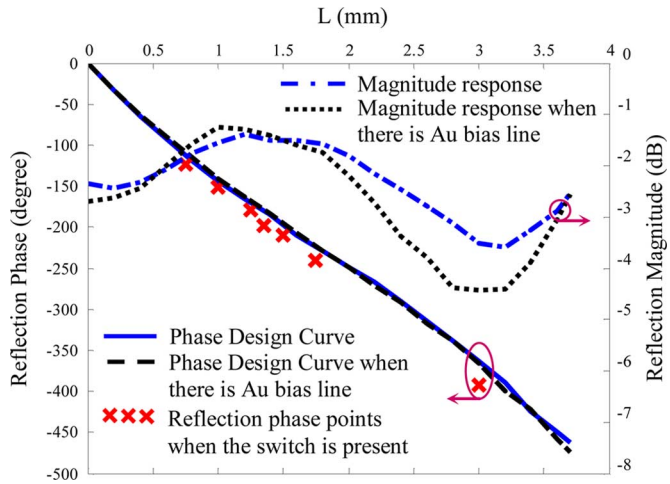

Fig. 7. The effect of the Au bias lines and the RF MEMS switch on both the reflection phase and magnitude curves at 26.5 GHz.

have no significant effect on the phase design curve but the amplitude of the reflected wave decreases for some values of L.

The phase design curve given in Fig. 2 is obtained by changing the length of the microstrip line. To calculate the reflection phase more realistically, the unit cell is simulated by including the series RF MEMS switch. Fig. 7 shows the reflection phase values of the reconfigurable unit cell calculated both for different L_{i1}, L_{i3} values and for the up or down states of the switch [15], which are seen to be slightly deviating from the phase design curve. Hence, L_{i1}, L_{i3} values determined from the phase design curve in Section II are altered for the fine tuning of the phases.

IV. Fabrication of Reconfigurable Reflectarray

The monolithic reconfigurable reflectarray presented in this work is produced using the surface micromachining based process including the wafer bonding step developed at Middle East Technical University MEMS Center (METU-MEMS Center). Fig. 6 shows the layout of the reconfigurable reflectarray. The reflectarray has been fabricated using two 500 μm thick glass substrates ($\varepsilon_r = 4.6$, $\tan\delta = 0.005$). Fig. 8 shows a simplified process flow. Fig. 8(a) shows a cross-sectional view of the process which can be obtained after a number of process steps. The process starts by coating each wafer with a 100/8000 Å thick Ti/Au layer and patterning by wet etching to construct the aperture on the ground plane. Then, both wafers are bonded using gold-to-gold thermal compression bonding at 265 °C for 1 hour in a vacuum to construct a common ground plane with the aperture. Next, one side of the bonded glasses is processed to have the microstrip patch antenna, whereas the other side is used to construct the transmission lines with the RF MEMS switches. The microstrip patch antenna is constructed by sputtering and patterning a 100/8000 Å thick Ti/Au layer. The process at the other side of the bonded glasses starts with a 2000 Å thick Si-Cr resistive layer deposition by sputtering and then patterning by wet etching. After that, the patch antennas are covered with a 0.8 μm thick sputtered Ti layer to protect them while processing the other side of the wafer. The next step is the sputtering of a 100/6000 Å thick Ti/Au layer on the Si-Cr resistive layer; after wet etching, the

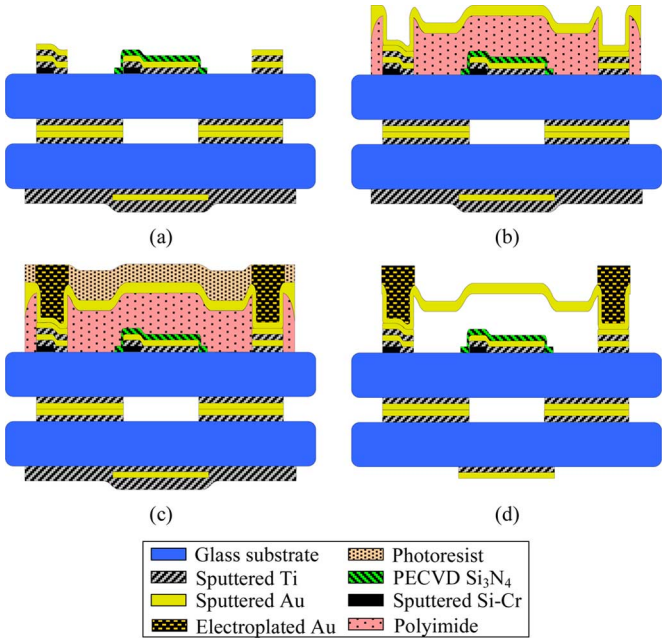

Fig. 8. The standard process flow developed at METU-MEMS Center for the production of the reconfigurable reflectarray.

transmission lines are formed. Then, again a 100/2500 Å thick Ti/Au layer is sputtered on the whole wafer area covering the previously formed transmission lines. After wet etching of this layer, the actuation pads are formed, and the height of the transmission lines is increased with respect to the actuation pads, which helps to decrease the contact resistance of the series RF MEMS switch. Then, a 3000 Å thick Si_3N_4 layer is coated as a DC isolation layer using the plasma enhanced chemical vapor deposition (PECVD) technique and patterned using the reactive ion etching (RIE) technique, resulting in the structure shown in Fig. 8(a). Fig. 8(b) shows the cross-section after the photo definable polyimide, PI 2737, is spin-coated to form a 2 μm thick sacrificial layer and patterned to obtain hollows for the anchor regions, which is followed by sputtering a 1 μm thick gold layer on the PI 2737. Fig. 8(c) shows the cross-section after the anchors are strengthened with a 2 μm thick electroplated gold layer inside the regions defined by a mold photoresist. Then, the photoresist is removed, the structural layer is patterned, and the Ti layer used to protect the patch antennas is removed by wet etching. Fig. 8(d) shows the final cross-section after the sacrificial layer is removed by wet etching in an EKC-265 solution, and the wafer is rinsed in IPA and dried in a supercritical point dryer. Fig. 9 shows the photographs of the fabricated reflectarray, while Fig. 10 shows the optical and SEM photographs of the series RF MEMS switch monolithically integrated to the reflectarray.

Although the individual process steps are easy, it is a challenge to obtain the whole reflectarray on a 4″ wafer, as the reflectarray covers nearly the whole area of the 4″ wafer and as the monolithic integration requires a high yield of RF MEMS switches distributed over the large wafer area. After a number of trials and process improvements, a high yield process is achieved to obtain a working reflectarray.

The size of the reflectarray is 6.75 cm × 6.29 cm. It is centered on the wafer. Individual RF MEMS switches are located on the

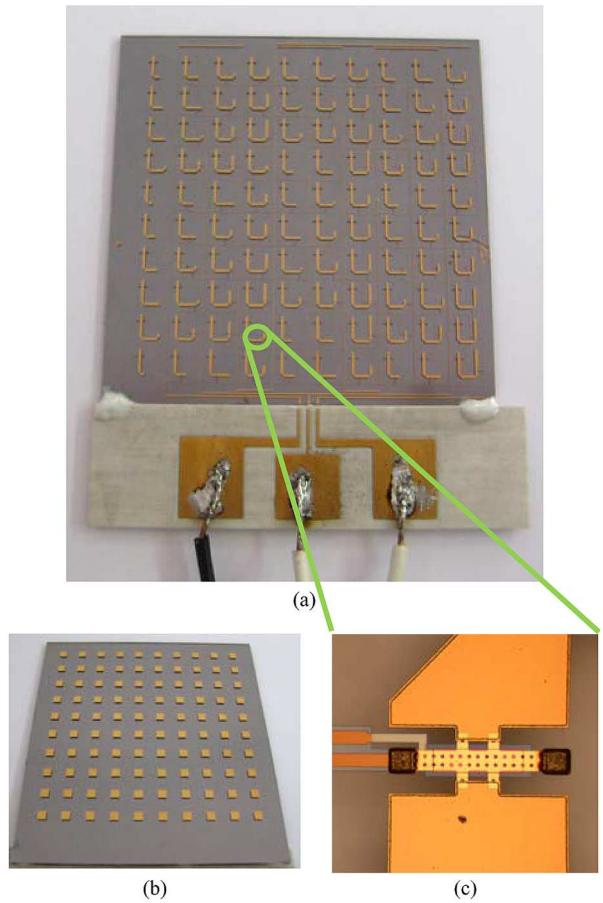

Fig. 9. (a) Transmission line and (b) patch antenna side of the reconfigurable reflectarray antenna monolithically produced with (c) the series RF MEMS switches.

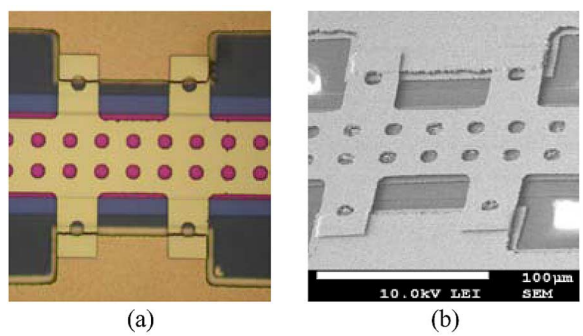

Fig. 10. (a) Microscopy and (b) SEM views of the series RF MEMS switch monolithically produced with the reflectarray.

rest of the wafer area. The actuation voltage of these switches is measured as 35 V. Since the electroplating thickness is not uniform over the wafer (it increases toward the edge), it is expected that the actuation voltage of the switches in the reflectarray region is less than 35 V. Hence, 35 V is used as the actuation voltage in the measurements.

V. Simulation and Measurement Results

The simulations of the full reflectarray, i.e., the reflectarray surface and the feed horn, are carried out in HFSS to compare with the measurements. First of all, up and down states of the series RF MEMS switches in the reflectarray are modeled and

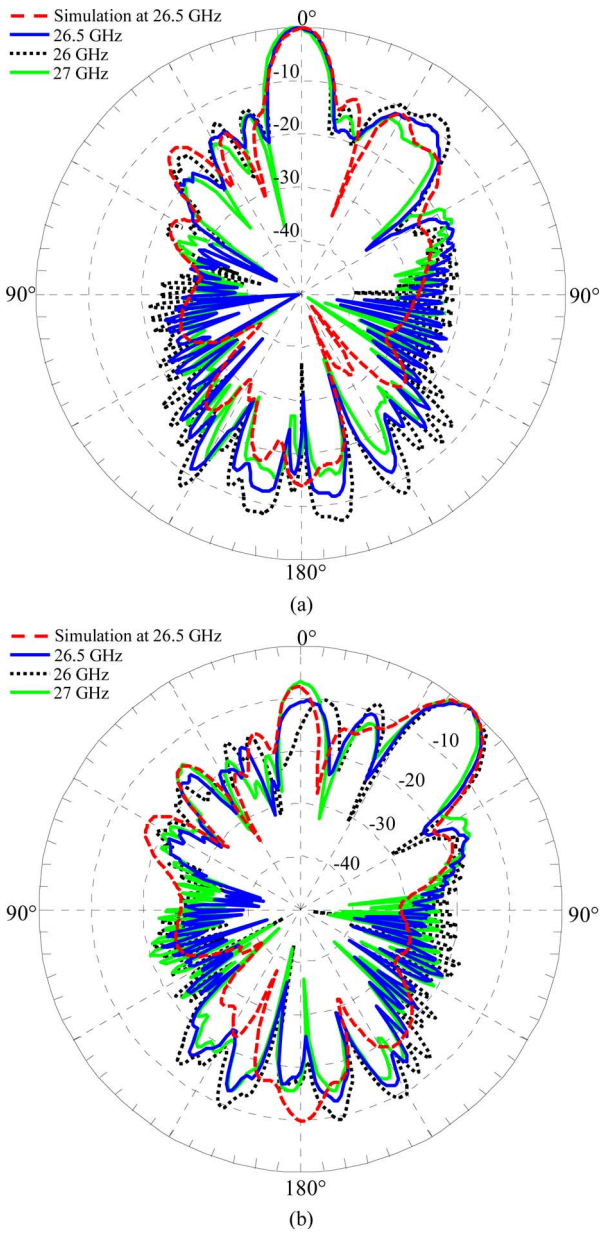

Fig. 11. The measured radiation patterns and simulation results in the H-plane. (a) When the switches are actuated to direct the main beam to the broadside. (b) When the switches are actuated to direct the main beam to 40°.

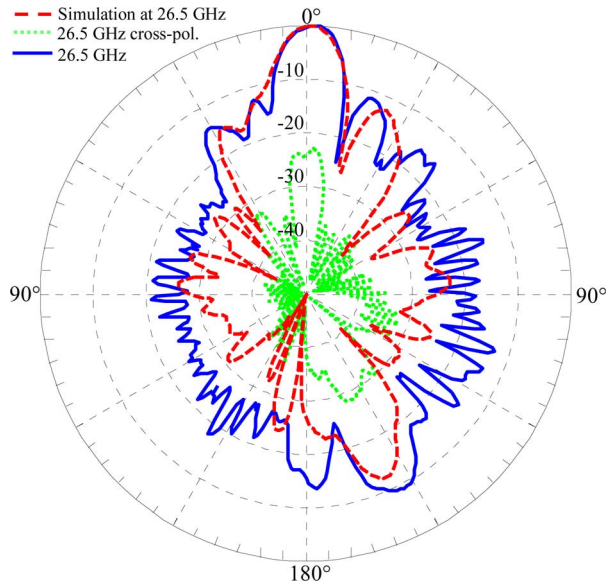

Fig. 12. The measured radiation patterns in the E-plane when the switches are actuated to direct the main beam to 40° and the simulation result.

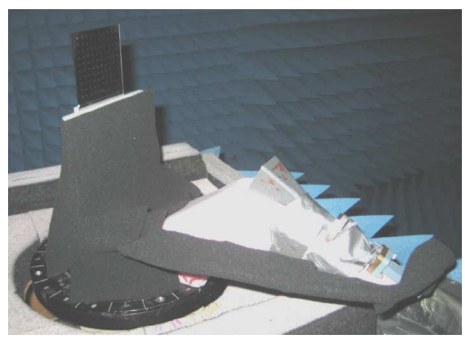

Fig. 13. The measurement setup of the reconfigurable reflectarray.

replaced by series capacitances and inductances. Since the reflectarray together with the feed horn antenna is a very large structure with respect to the wavelength, the problem is divided into two parts: the feed horn region and the reflectarray surface. Then, these two parts are related with an HFSS data-link. First, the near field of the feed horn antenna is calculated by simulations. Then, this near field is taken as the incident field that illuminates the reflecting surface by using the data-link tool. Figs. 11 and 12 show the full wave EM simulation plots of the far fields, in addition to measurement results, as explained later.

To prepare the antenna for the measurements, a PCB card is attached to the fabricated reflectarray to apply the DC bias voltage to the switches, as shown in Fig. 9(a). Three wire bonds are taken from the reflectarray to the PCB card to achieve the DC connections to the pads *GND*, *SIGNAL1*, *SIGNAL2* shown in Fig. 6. The reflectarray and offset feed horn are assembled on the foam support structure such that the position of the phase center of the feed horn antenna with respect to the center of the reflectarray is as indicated in Section II. Fig. 13 shows a photograph of the complete antenna placed in an anechoic chamber. All the pattern measurements are taken with a 1° angular resolution. When the actuation voltage is applied between *GND* and *SIGNAL2*, the main beam of the reflectarray is directed to the broadside as shown in Fig. 11(a); the half power beam width is determined to be 10°. When the actuation voltage is applied between *GND* and *SIGNAL1*, the main beam of the reflectarray is switched to 40° in the H-plane as shown in Fig. 11(b) with the half power beam width of 13°. The measured radiation and cross polarization patterns in the E-plane for the 40° operation are presented in Fig. 12. The measured cross polarization level in the E-plane is found to be better than −20 dB. The measurement results given in Fig. 11 show that there are abrupt changes especially in the angular region approximately between 90° and 140° where the field is below −20 dB, due to non-ideal characteristics of the rotary joint of the measurement setup at this frequency range. It is observed from Figs. 11 and 12 that, there is a good agreement between the measurement and simulation results. The positions of the main beam, half power beam width,

TABLE I
LOSS ANALYSIS FOR 40° OPERATION AT 26.5 GHZ

Quantity	Value	
Gain	11.42 dB	(Measured)
Directivity	22.47 dB	(Calculated)
Efficiency	7.85%	
Directivity-Gain (Measured Loss)	11.05 dB	
Spillover Loss	6.51 dB	(Calculated)
Taper Loss	0.0064 dB	(Calculated)
Cross Pol. Loss	0.15 dB	(Calculated)
Maximum Element Reflectivity Loss	3.64 dB	(Calculated)
Insertion Loss of RF MEMS switch	0.3 dB	(Calculated)
Total Calculated Loss	10.61 dB	
Measured Loss - Total Calculated Loss	0.44 dB	

side lobe levels, and back radiation levels in the simulation are nearly the same for both the broadside and 40° operations. The slight deviations in the positions of the side and back lobes and the levels of some side lobes are mainly caused by the differences between the simulation and the measurement setup. The actual interaction of the horn antenna and the reflectarray cannot be fully taken into account in the simulations due to the very large electrical size of the overall antenna. Moreover, the coaxial cable and the connector used to excite the horn antenna are not included in the simulations.

The maximum back radiation and side lobe levels are around -12 dB, and -10 dB, respectively. This reflectarray is a proof-of-concept prototype, and the main goal is to demonstrate the beam switching by an RF MEMS switch control. Thus, in the design, no special efforts have been spent to reduce the side lobe levels and back radiation. To reduce the back radiation, a ground plane can be placed at an appropriate distance from the back side of the reflectarray.

When we consider both the broadside and 40° operations, the maximum value of the side lobe levels is around -7 dB and the maximum deviation in both the half power beam width (HPBW) values and the main beam directions is 1° within the 26–27 GHz frequency band. These values are acceptable within 26–27 GHz, and hence, the bandwidth is 3.77%.

A loss analysis of the reflectarray is performed when the main beam is directed to 40° and tabulated in Table I. The gain of the reflectarray is measured as 11.42 dBi by using a standard gain horn antenna at 26.5 GHz, whereas the gain is calculated as 11.93 dBi using the simulation results. The directivity of a 10×10 uniform array radiating to 40° is calculated numerically as 22.47 dB. Using the measured gain, total loss of the reflectarray is estimated as 11.05 dB which corresponds to an antenna efficiency of 7.85%.

Illumination, cross polarization, and element losses are calculated numerically at 26.5 GHz. The main loss source is the spillover loss, which is calculated as 6.51 dB. The taper loss is 0.0064 dB, which is very small, because the illuminating horn antenna has high HPBW values of 34° in the H-plane and 26° in the E-plane, resulting in an almost uniform illumination and a high spillover loss. By optimizing the focal distance/diameter (F/D) ratio, the spillover loss can be reduced. The cross polarization loss is calculated as 0.15 dB. The maximum element reflectivity loss is 3.64 dB at the normal plane wave incidence, but it can be reduced by placing an additional ground plane at the back side of the array. The 0.3 dB insertion loss of the series RF MEMS switch also contributes to the total loss of the reflectarray. Calculated losses in Table I add up to 10.61 dB. The difference between the calculated and measured loss (0.44 dB) might be caused by several factors, including small errors in the placement of the phase center of the feed horn at the focal point of the reflectarray. Furthermore, the ohmic losses are ignored in the reflectarray radiation pattern simulations, i.e., all the metals in the full reflectarray structure are assumed to be perfectly conducting and second order interactions of reflecting surface with the horn are not taken into account in the simulations.

The good agreement between the simulation and measurement results shows that almost all of the switches on the reflectarray are fully functional, i.e., the yield is very high. The yield is estimated as 88% based on the surface profile measurements of the reflectarray and RF measurements of the individual RF MEMS switches from the same wafer.

VI. CONCLUSION

Beam switching of a 26.5 GHz 10×10 reconfigurable reflectarray antenna is achieved using 90 RF MEMS switches in the ACMPA elements. The progressive phase shift between the elements is adjusted by the on and off state positions of the series RF MEMS switches inserted in the transmission line of the ACMPA elements. The full reflectarray is produced monolithically with the series RF MEMS switches. Measurement results demonstrate that the main beam of the reflectarray can be switched between the broadside and 40° by the help of the RF MEMS switches. According to the authors' knowledge, this monolithically integrated MEMS reconfigurable reflectarray is the first functional prototype that employs a large number of RF MEMS switches distributed over a large wafer area, demonstrating the potential of the RF MEMS technology for large scale antennas.

ACKNOWLEDGMENT

The authors would like to thank METU-MEMS Center staff of Middle East Technical University, Ankara, Turkey, for their support in the fabrication. The authors also thank Dr. Kagan Topalli and Dr. Mehmet Unlu for the development of the process and their supervision in the fabrication.

REFERENCES

[1] D. M. Pozar, S. D. Targonski, and H. D. Syrigos, "Design of millimeter wave microstrip reflectarrays," *IEEE Trans. Antennas Propag.*, vol. 45, no. 2, pp. 287–296, Feb. 1997.

[2] J. Huang and J. Encinar, *Reflectarray Antennas*. Piscataway, NJ: Wiley-IEEE Press, 2007.

[3] T. Metzler and D. Schaubert, "Scattering from a stub loaded microstrip antenna," in *IEEE Antennas and Propagation Society Int. Symp., AP-S. Dig.*, Jun. 1989, pp. 446–449.

[4] D. M. Pozar and S. D. Targonski, "A microstrip reflectarray using crossed dipoles," in *IEEE Antennas and Propagation Society Int. Symp., AP-S. Dig.*, Jun. 1998, pp. 1008–1011.

[5] J. A. Encinar, "Design of two-layer printed reflectarrays using patches of variable size," *IEEE Trans. Antennas Propag.*, vol. 49, no. 10, pp. 1403–14010, Oct. 2001.

[6] A. Mössinger, R. Marin, S. Mueller, J. Freese, and R. Jakoby, "Electronically reconfigurable reflectarrays with nematic liquid crystals," *IEE Electron. Lett.*, vol. 42, pp. 899–900, Aug. 2006.

[7] W. Hu, M. Y. Ismail, R. Cahill, J. A. Encinar, V. F. Fusco, H. S. Gamble, R. Dickie, D. Linton, N. Grant, and S. P. Rea, "Electronically reconfigurable monopulse reflectarray antenna with liquid crystal substrate," in *Proc. 2nd EuCAP*, Edinburgh, U.K., Nov. 11–16, 2007, pp. 1–6.

[8] F. Venneri, L. Boccia, G. Angiulli, G. Amendola, and G. Di Massa, "Analysis and design of passive and active microstrip reflectarrays," *Int. J. RF Microw. Comput.-Aid. Eng.*, vol. 13, pp. 370–377, 2003.
[9] D. F. Sievenpiper, J. H. Schaffner, H. J. Song, R. Y. Loo, and G. Tangonan, "Two-dimensional beam steering using an electrically tunable impedance surface," *IEEE Trans. Antennas Propag.*, vol. 51, no. 10, pt. 1, pp. 2713–272, Oct. 2003.
[10] M. Riel and J.-J. Laurin, "Design of an electronically beam scanning reflectarray using aperture-coupled elements," *IEEE Trans. Antennas Propag.*, vol. 55, no. 5, pp. 1260–1266, May 2007.
[11] M. Hajian, B. Kuijpers, K. Buisman, A. Akhnoukh, M. Plek, L. C. N. de Vreede, J. Zijdeveld, and L. P. Ligthart, "Active scan-beam reflectarray antenna loaded with tunable capacitor," in *Proc. 3rd EuCAP*, Berlin, Germany, Mar. 23–27, 2009, pp. 1158–1161.
[12] S. V. Hum, M. Okoniewski, and R. J. Davies, "Modeling and design of electronically tunable reflectarrays," *IEEE Trans. Antennas Propag.*, vol. 55, no. 8, pp. 2200–2210, Aug. 2007.
[13] H. Kamoda, T. Iwasaki, J. Tsumochi, and T. Kuki, "60-GHz electrically reconfigurable reflectarray using p-i-n diode," in *IEEE Microwave Symp. Dig.*, Jun. 2009, pp. 1177–1180.
[14] J. Perruisseau-Carrier, "Dual-polarized and polarization-flexible reflective cells with dynamic phase control," *IEEE Trans. Antennas Propag.*, vol. 58, no. 5, pp. 1494–1502, May 2010.
[15] O. Bayraktar, K. Topalli, M. Unlu, O. A. Civi, S. Demir, and T. Akin, "Beam switching reflectarray using RF MEMS technology," in *Proc. 2nd EuCAP*, Edinburgh, U.K., Nov. 11–16, 2007, pp. 1–6.
[16] J. Huang, "Analysis of a Microstrip Reflectarray Antenna for Microspacecraft Applications," NASA TDA progress report, Feb. 1995, pp. 153–173.
[17] R. J. Richards, E. W. Dittrich, O. B. Kesler, and J. M. Grimm, "Microstrip Phase Shifting Reflect Array Antenna," U.S. Patent 6,020,853, Feb. 1, 2000.
[18] R. J. Richards, "Integrated Microelectromechanical Phase Shifting Reflect Array Antenna," U.S. Patent 6,195,047, Feb. 27, 2001.
[19] H. Legay, B. Pinte, M. Charrier, A. Ziaei, E. Girard, and R. Gillard, "A steerable reflectarray antenna with MEMS controls," in *Proc. IEEE Int. Symp. Phased Array Systems and Tech.*, Oct. 14–17, 2003, pp. 494–499.
[20] C. Guclu, J. Perruisseau-Carrier, and O. A. Civi, "Dual frequency reflectarray cell using split-ring elements with RF MEMS switches," in *Proc. IEEE Int. Symp. Antennas and Propagation and USNC/URSI National Radio Science Meeting*, Toronto, ON, Canada, Jul. 11–17, 2010, pp. 1–4.
[21] R. Gilbert, "Dipole Tunable Reconfigurable Reflector Array," U.S. Patent 6,426,727, Jul. 30, 2002.
[22] H. P. Hsu and T. Y. Hsu, "Optically Controlled RF MEMS Switch Array for Reconfigurable Broadband Reflective Antennas," U.S. Patent 6,417,807, Jul. 9, 2002.
[23] J. Perruisseau-Carrier and A. K. Skrivervik, "Monolithic MEMS-based reflectarray cell digitally reconfigurable over a 360° phase range," *IEEE Antennas Wireless Propag. Lett.*, vol. 7, pp. 138–141, 2008.
[24] S. V. Hum, G. McFeetors, and M. Okoniewski, "Integrated MEMS reflectarray elements," in *Proc. 1st EuCAP*, Nice, France, Nov. 6–10, 2006, pp. 1–6.
[25] L. Marcaccioli, B. Mencagli, R. V. Gatti, T. Feger, T. Purtova, H. Schumacher, and R. Sorrentino, "Beam steering MEMS mm-wave reflectarrays," in *Proc. 7th Int. Symp. RF MEMS and RF Microsystems (MEMSWAVE 2006)*, Orvieto, Italy, Jun. 27–30, 2006.
[26] B. Mencagli, R. V. Gatti, L. Marcaccioli, and R. Sorrentino, "Design of large mm-wave beam-scanning reflectarrays," in *Proc. 35th EuMC*, Paris, France, Oct. 3–7, 2005.
[27] C. C. Cheng, B. Lakshminarayanan, and A. Abbaspour-Tamijani, "A programmable lens array antenna with monolithically integrated MEMS switches," *IEEE Trans. Microw. Theory Tech.*, vol. 57, no. 8, pp. 1874–1884, Aug. 2009.
[28] G. M. Rebeiz, K. Entesari, I. C. Reines, S. J. Park, M. A. El-Tanani, A. Grichener, and A. R. Brown, "Tuning in to RF MEMS," *IEEE Microw. Mag.*, pp. 55–72, Oct. 2009.
[29] H. Salti, E. Fourn, R. Gillard, and H. Legay, "Minimization of MEMS breakdowns effects on the radiation of a MEMS based reconfigurable reflectarray," *IEEE Trans. Antennas Propag.*, vol. 58, no. 7, pp. 2281–2287, Jul. 2010.
[30] J. A. Encinar and J. A. Zornoza, "Broadband design of three-layer printed reflectarrays," *IEEE Trans. Antennas Propag.*, vol. 51, pp. 1662–1664, Jul. 2003.

Omer Bayraktar was born in Aydin, Turkey, in 1983. He received the B.Sc. and M.Sc. degrees in electrical and electronics engineering from the Middle East Technical University (METU), Ankara, Turkey, in 2005 and 2007, respectively.

Since 2005, he has been working as a research assistant at METU in the Department of Electrical and Electronics Engineering. His major research interests include development, characterization, and integration of novel RF MEMS structures such as switches, phase shifters for RF front-ends at microwave and millimeter-wave, reconfigurable antennas, phased arrays, and reflectarrays.

Özlem Aydin Civi (S'90–M'97–SM'05) received the B.Sc., M.Sc., and Ph.D. degrees in electrical and electronics engineering in 1990, 1992, and 1996, respectively, at the Middle East Technical University (METU), Ankara, Turkey.

She was a research assistant in METU from 1990 to 1996. In 1997–1998, she was a visiting scientist at the ElectroScience Laboratory, Ohio State University. Since 1998, she has been with the Department of Electrical and Electronics Engineering, METU, where she is currently a Professor. Her research interests include analytical, numerical and hybrid techniques in EMT problems, especially fast asymptotic/hybrid techniques for the analysis of large finite periodic structures, multi-function antenna design, reconfigurable antennas, phased arrays, reflectarrays and RF-MEMS applications. Since 1997, she has been a national delegate of the European actions COST260, COST284, COST-IC0603 on antennas. She is a technical reviewer of the European Community for scientific projects in the fields of antennas and communication. She has published over 100 journal and international conference papers.

Dr. Civi was a recipient of the 1994 Prof. Mustafa Parlar Foundation Research and Encouragement award with METU Radar Group and the 1996 URSI Young Scientist Award. She was the chair of the IEEE Turkey Section in 2006 and 2007, and the chair of the IEEE AP/MTT/ED/EMC Chapter between 2004 and 2006. She is a member of the Administrative Committee of the Turkish National Committee of URSI. She is an Associate Editor of the IEEE TRANSACTIONS ON ANTENNAS AND PROPAGATION.

Tayfun Akin (S'90–M'97) was born in Van, Turkey, in 1966. He received the B.S. degree in electrical engineering with high honors from Middle East Technical University, Ankara, Turkey, in 1987, and went to the USA in 1987 for his graduate studies with a graduate fellowship provided by NATO Science Scholarship Program through the Scientific and Technical Research Council of Turkey (TUBITAK). He received the M.S. degree in 1989 and the Ph.D. degree in 1994 in electrical engineering, both from the University of Michigan, Ann Arbor.

He became an Assistant Professor in 1995, an Associate Professor in 1998, and Professor in 2004 in the Department of Electrical and Electronics Engineering at Middle East Technical University, Ankara, Turkey. He is also the Director of the METU-MEMS Center which has a 1300 m^2 clean room area for MEMS process and testing. His research interests include MEMS, microsystems technologies, infrared detectors and readout circuits, silicon-based integrated sensors and transducers, and analog and digital integrated circuit design.

Dr. Akin has served in various MEMS, EUROSENSORS, and TRANSDUCERS conferences as a Technical Program Committee Member. He was the co-chair of the 19th IEEE International Conference of Micro Electro Mechanical Systems (MEMS 2006) held in Istanbul, and he was the co-chair of the Steering Committee of the IEEE MEMS Conference in 2007. He is the winner of the First Prize in Experienced Analog/Digital Mixed-Signal Design Category at the 1994 Student VLSI Circuit Design Contest organized and sponsored by Mentor Graphics, Texas Instruments, Hewlett-Packard, Sun Microsystems, and Electronic Design Magazine. He is a co-author of the symmetric and decoupled gyroscope project which won the first prize in the operational designs category of the international design contest organized by DATE Conference and CMP in March 2001. He is also the co-author of the gyroscope project which won the third prize of the 3-D MEMS Design Challenge organized by MEMGen (currently Microfabrica).